Liquid Crystals
Publication details, including instructions for authors and subscription information:
http://www.informaworld.com/smpp/title~content=t713926090

Twisted grain boundary phases in three new chiral azobenzene series

M. Werth[a]; H. T. Nguyen[a]; C. Destrade[a]; N. Isaert[b]
[a] Centre de Recherche Paul Pascal, Pessac, Cedex, France [b] Laboratoire de Dynamique et Structure des Matériaux Moléulaires (U.R.A, CNRS No. 801), Université de Lille 1, Villeneuve d'Ascq Cedex, France

To cite this Article Werth, M. , Nguyen, H. T. , Destrade, C. and Isaert, N.(1994) 'Twisted grain boundary phases in three new chiral azobenzene series', Liquid Crystals, 17: 6, 863 — 877
To link to this Article: DOI: 10.1080/02678299408035479
URL: http://dx.doi.org/10.1080/02678299408035479

LIQUID CRYSTALS, 1994, VOL. 17, NO. 6, 863–877

Twisted grain boundary phases in three new chiral azobenzene series

by M. WERTH†, H. T. NGUYEN*, C. DESTRADE
Centre de Recherche Paul Pascal, Av. A. Schweitzer,
F33600 Pessac Cedex, France

and N. ISAERT
Laboratoire de Dynamique et Structure des Matériaux Moléculaires
(U.R.A, CNRS No. 801), Université de Lille 1, U.F.R. de Physique,
F 59655 Villeneuve d'Ascq Cedex, France

(Received 8 March 1994; accepted 25 April 1994)

Three new chiral series with an azobenzene core have been synthesized and studied. The twist grain boundary smectic A and C phases, obtained with a cholesteric texture, were characterized by different techniques: binary diagram, racemic mixtures, helical pitch measurement and X-ray diffraction. Helical pitch measurements of the TGB_A and TGB_C phases were performed using Grandjean–Cano wedges and those of the S_C^* phase with homeotropic drops. The pitch values are similar to those of tolane compounds previously studied. Electro-optical properties of the S_C^* phase were measured with classical SSFLC geometry and the results are comparable with previous studies.

1. Introduction

During the past years, studies on the frustrated phases of chiral molecules on their transition from the helical smectic C* or smectic A phases to the cholesteric or isotropic phases have intensified. These phases were first predicted in 1972 by de Gennes [1] from an analogy between the nematic to smectic A transition and the normal to superconductor transition in metals. These phases reflect the antagonism between the non-centrosymmetrical-helical-superstructure, which is a direct consequence of the non-centrosymmetrical-chiral-molecular structure, and the layered structure of the smectic phases.

The theoretical structures of these new phases were proposed in 1988 by Renn and Lubensky [2]: two-dimensional slabs of the smectic phase are arrayed along a helix axis parallel to the smectic layers. Adjacent slabs are separated by grain boundaries which consist of a grid of parallel equispaced screw dislocation lines to allow for the helical twist—hence the name 'twisted grain boundary phases' (TGB). The authors also proposed that three helical analogues of the smectic A, smectic C and helical smectic C* phase should exist [3, 4].

By now, the analogues of the smectic A and the smectic C phases have been found in varying phase sequences [5, 6, 7]. Here the phase sequence $S_C^* S_A TGB_A N^*$ is of

* Author for correspondence.
† Present address: CERDATO, F27470 Serquigny, France.

0267–8292/94 $10·00

special importance as it provides the theoretical connection to the tricritical NAC point [8]. In this article we present a study of the structural variation of molecules which may constitute a TGB phase. In general, these molecules have three aromatic rings with an additional acetylenic group placed between two rings which makes the molecular core rather elongated and rigid. In addition the chiral centre is placed at the molecular head with a moderate dipole pointing in its direction [9].

Inspired by the very similar molecular and crystal structures of tolane and azobenzene systems [10], we have now performed the synthesis and phase characterization of three new mesogenic series where the acetylenic moiety is replaced by an azo-group. The three series differ in the number of laterally attached fluorines which have been shown to induce remarkable effects on the mesomorphic properties, in particular concerning the TGB phases in the tolanes [8, 9].

Because of the relative ease of synthesis of azo-compounds, this molecular class seemed to us a promising candidate to extend the pool of molecules exhibiting TGB phases. In addition, it allows for a different chemistry, in particular when one is seeking mesomorphic polymers, and it introduces colour into the compounds.

In the following sections we will describe the synthesis (§2), the mesomorphic properties (§3), X-ray structural investigations (§4), helical pitch measurements (§5) and electro-optical measurements (§6). In a summarizing discussion we will compare the azobenzenes in their phase behaviour and electro-optic properties with the well-known tolane compounds.

2. Synthesis

The compounds of the series *n*A, *n*FA and *n*F_2A were prepared according to the following scheme:

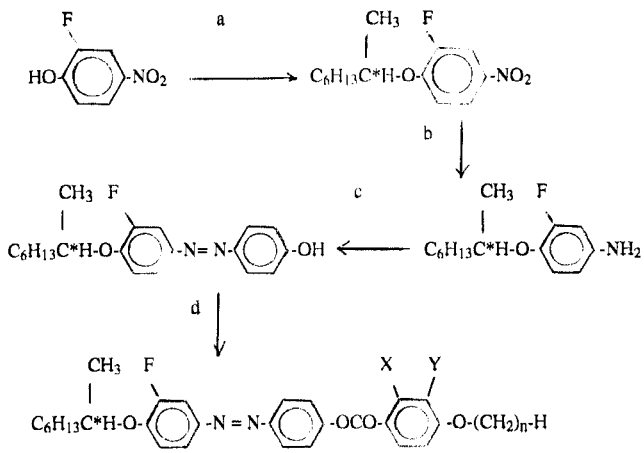

where $X = Y = H$: *n*A series, $X = H$, $Y = F$: *n*FA series, $X = Y = F$: *n*F_2A series, and *n* corresponds to the length of the terminal alkyl chain.

(*a*) (*R*)–$C_6H_{13}C^*H(CH_3)$–OH, Ph_3P, DEAD, CH_2Cl_2.
(*b*) H_2, Pd(C) 10 per cent, EtOAc.
(*c*) (1) HCl dil., dioxan, $NaNO_2$; (2) phenol, NaOH aq.

(*d*) 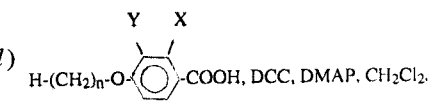

The synthesis of the substituted benzoic acids is described elsewhere [11, 12]. All final compounds were purified by column chromatography on silica gel using toluene as eluent, with subsequent recrystallization from ethanol. Elementary analysis and ^{1}H NMR spectra gave satisfactory results in all cases. Details of the synthesis are reported in the experimental section.

3. Mesomorphic properties

All compounds studied are mesomorphic. For the microscopic observations we used a Zeiss Ortholux equipped with a Mettler FP 5 hot stage and for the calorimetric studies a Perkin–Elmer DSC 7 was used. Usual heating rates were $4° \min^{-1}$ over larger temperature intervals and 1 or $2° \min^{-1}$ in the TGB range.

3.1. *Microscopic observations*

When cooling from the isotropic phase, most often two blue phases appear. Only for the higher homologues of the *n*A and *n*FA series are there no blue phases, and the transition occurs directly into a TGB or smectic phase. Blue phase II can be seen by the colour change to a dark blue to green and blue phase I shows a characteristic grazed platelet texture which can be supercooled up to 4°. Then the cholesteric Grandjean plane texture appears which, on temperature changes, shows strong undulations. In the case where a TGB phase exists, a slight colour change to a brownish-red can be observed at the transition and the Grandjean plane texture becomes more viscous and blurred. On further cooling from either the TGB (TGB_A or TGB_C) or the cholesteric phase, the transition to a smectic phase takes place with the appearance of dechiralization lines. The smectic A phase shows a characteristic focal-conic texture with large homeotropic regions. Often a 'noyaux' texture is observed at higher temperatures, too. The helical smectic C* phase, too, exhibits a broken fan-shaped texture with large pseudo-homeotropic domains. Transitions between the smectic A and the helical smectic C* phases are very difficult to see due to the close resemblance of their textures.

The final assignment of the phases, especially the nature of the TGB phase, was based upon a combination of DSC, studies of racemic mixtures, contact preparations, miscibility studies with known compounds, helical pitch measurements, X-ray diffraction and a characterization of the electro-optical properties. The plots of the transition temperatures of the *n*A, *n*FA and *n*F_2A compounds against *n*, the number of carbon atoms in the aliphatic chain, are given in figures 1, 2 and 3.

3.2. *Calorimetric studies*

In tables 1, 2 and 3, the transition temperatures and the transitional heats are given as they were obtained on heating. Very often a solid polymorphism is encountered which can also be observed under the microscope. The melting temperatures given are therefore only the highest temperatures before entering a smectic phase and also the heats of fusion are those of the highest peaks. With increasing chain lengths, the transitions between the smectic, TGB and cholesteric phases and the transitions between the cholesteric, blue and isotropic phases superimpose. In those cases the sum of the heats of the transition is always given. Generally it can be noticed that the heats of transition of the smectic C to A transition and of the smectic to TGB phase transition

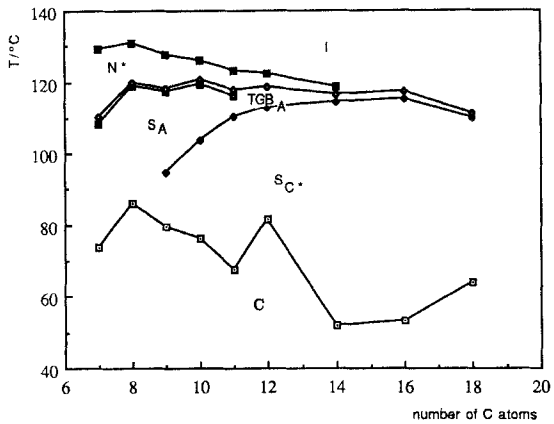

Figure 1. Plots of the transition temperatures of the *n*A compounds against *n*, the number of carbon atoms of the aliphatic chain.

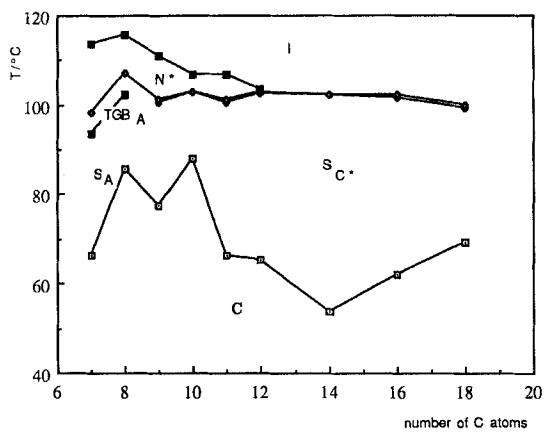

Figure 2. Plots of the transition temperatures of the *n*FA compounds against *n*, the number of carbon atoms of the aliphatic chain.

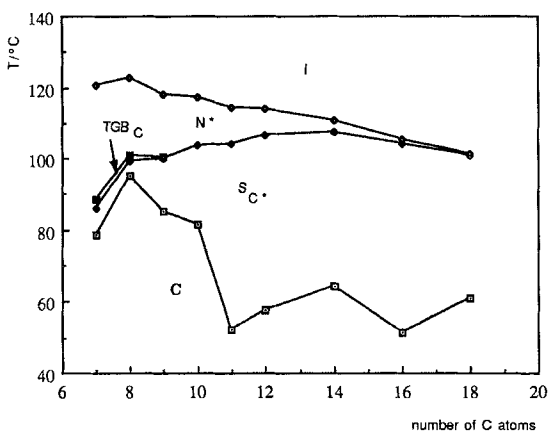

Figure 3. Plots of the transition temperatures of the nF_2A compounds against *n*, the number of carbon atoms of the aliphatic chain.

Table 1. Transition temperatures (°C) and enthalpies in italics (kJ mol^{-1}) for the *n*A compounds.

	C		S_C^*		S_A		TGB_A		N*		BP		I
7A	•	73·9	—		•	108·5	•	110·5	•	129·5	•	131·0	•
		23·3					*0·37*†				*0·72*†		
8A	•	85·9	—		•	119·0	•	120·0	•	131·0	•	132·5	•
		36·4					*0·51*†				*0·71*†		
9A	•	79·7	•	94·7	•	117·2	•	118·2	•	127·7	•	128·6	•
		34·0		*0·02*			*0·42*†				*0·71*†		
10A	•	76·4	•	103·6	•	119·3	•	120·6	•	125·9	•	127·0	•
		29·7		*0·02*			*0·58*†				*0·94*†		
11A	•	67·7	•	110·3	•	116·3	•	117·7	•	123·0	•	124·1	•
		36·0		*0·04*			*0·41*†				*0·92*†		
12A	•	81·5	•	113·4	—		•	118·4	•	122·3	•	123·2	•
		53·2		*0·10*				*0·44*†			*1·41*†		
14A	•	52·0	•	114·5	—		•	116·4	•	118·5	•	119·4	•
		39·5		*0·26*				*2·73*†					
16A	•	53·2	•	115·2	—		•	117·4	—		—		•
		40·7						*4·84*†					
18A	•	64·0	•	109·9	—		•	111·1	—		—		•
		42·2						*5·15*†					

† Sum of transition enthalpies.

Table 2. Transition temperatures (°C) and enthalpies in italics (kJ mol^{-1}) for the *n*FA compounds.

	C		S_C^*		S_A		TGB_A		N*		BP		I
7FA	•	66·5	—		•	93·5	•	98·4	•	113·8	•	114·8	•
		30·5				*0·02*		*0·02*			*0·72*†		
8FA	•	85·9	—		•	102·3	•	107·1	•	115·6	•	116·8	•
		33·7				*0·01*		*0·37*			*0·94*†		
9FA	•	77·5	•	100·7	—		•	101·1	•	111·0	•	112·3	•
		36·8				*0·19*†					*0·98*†		
10FA	•	88·1	•	102·8	—		•	103·0	•	111·0	•	112·1	•
		54·8				*0·36*†					*1·07*†		
11FA	•	66·4	•	100·7	—		•	101·0	•	106·7	•	107·9	•
		45·8				*0·63*†					*1·15*†		
12FA	•	65·4	•	102·7	—		•	102·8	•	106·8	•	107·7	•
		33·73				*0·92*†					*1·48*†		
14FA	•	53·8	•	102·1	—		•	102·3	•	103·7	•	104·5	•
		48·8				*1·32*†					*1·78*†		
16FA	•	62·25	•	101·4	—		•	102·2	—		—		•
		53·5						*4·91*†					
18FA	•	69·25	•	99·4	—		•	99·9	—		—		•
		61·7						5·22†					

† Sum of transition enthalpies

Table 3. Transition temperatures (°C) and enthalpies in italics (kJ mol^{-1}) for the nF$_2$A compounds.

	C		S_C^*		TGB_C		N*		BP		I
7F$_2$A	•	78·5	•	86·0	•	88·5	•	120·5	•	121·9	•
		33·4		*0·01*		*0·13*			*0·43*†		
8F$_2$A	•	95·0	•	99·1	•	100·9	•	122·6	•	123·9	•
		41·5		*0·01*		*0·10*			*0·58*†		
9F$_2$A	•	85·2	•	100·0	•	100·5	•	118·3	•	119·5	•
		38·0			*0·28*†				*0·68*†		
10F$_2$A	•	81·5	•	103·8	—		•	117·5	•	118·8	•
		32·8			*0·39*†				*0·72*†		
11F$_2$A	•	52·5	•	104·2	—		•	114·3	•	115·6	•
		36·9		*0·64*					*0·90*†		
12F$_2$A	•	57·6	•	106·6	—		•	114·0	•	115·2	•
		43·5		*0·84*					*1·08*†		
14F$_2$A	•	64·1	•	107·4	—		•	110·7	•	111·6	•
		49·1		*1·33*					*1·39*†		
16F$_2$A	•	51·6	•	104·0	—		•	105·6	•	106·4	•
		46·7		*1·26*					*1·28*†		
18F$_2$A	•	61·0	•	100·9	—		•	101·5	•	102·3	•
		53·5					*4·27*†				

† Sum of transition enthalpies.

are extremely small. Typical thermograms are shown in figure 4 (*a*), (*b*), (*c*) in which only the transitions near the clearing point are given. The TGB_A–S_A and TGB_C– S_C^* are observed respectively, the first transition for the 8A, 8FA compounds and the latter for the 8F2A derivative. The sum of the heats of the smectic to cholesteric transitions augments with increasing chain length, and also the heat of the cholesteric to isotropic transition has an increasing tendency with lengthening chain before it reaches a plateau at long chain lengths, in contrast to the tolane series where these values remain approximately constant [7].

3.3. *Racemic systems and miscibility studies*

Racemic systems between the right-handed and the left-handed compounds were prepared, resulting in the following phase sequences observed by microscopy:

8A: C 69·3 S_A 121·0 N 132·0 I;
12A: C 72·5 S_C 113·5 S_A 119·0 N 123·9 I;
8FA: C 73·0 S_A 108·3 N 117·9 I;
12FA: C 51·0 S_C 103·4 N 108·9 I;
8F$_2$A: C 86·2 S_C 101·2 N 123·5 I;
10F$_2$A: C 73·5 S_C 103·6 N 119·0 I.

From these preparations, the TGB phase in the nA series is assigned as a TGB_A phase, whereas this is a TGB_C phase throughout the nF$_2$A series. Contact preparations confirmed the nature of the TGB phases of the remaining compounds. In the nFA series, we again encounter the TGB_A phase. However, the higher homologues with 10, 11 and 12 carbon chains have such small temperature intervals for the TGB phase that it is impossible to decide definitely on their exact nature.

Further miscibility studies with well-characterized, known compounds corroborated our phase designations. In figure 5 the miscibility diagram between (*S*)-7F$_2$A and

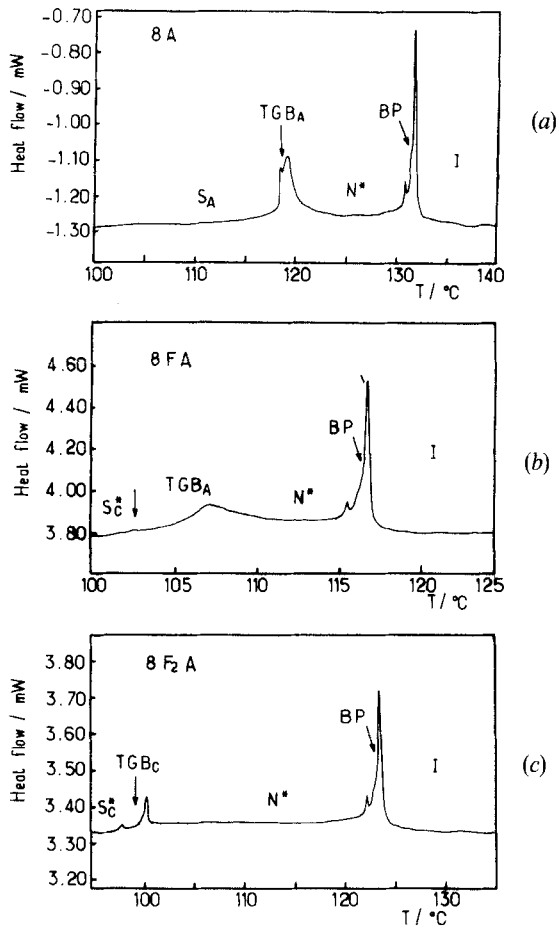

Figure 4. Differential scanning calorimetry thermogram with heating rate ($1^\circ min^{-1}$) for (*a*) 8A, (*b*) 8FA and (*c*) 8F2A.

(*S*)-12F_2BTFO$_1$M$_7$ is presented. The tolane compound (*S*)-12F_2BTFO$_1$M$_7$ has the following phase sequence [9]:

C 36·6 S_C^* 102·8 TGB_C 103·0 N* 110·5 BP 111·7 I.

The complete miscibility of the TGB phases, as well as of all other phases, is evident and confirms our assignment of the TGB_C phase. Moreover, the existence of chiral phases over the whole miscibility range confirms the existence of the same helical twist sense in both compounds. In figure 6 the binary phase diagram of the compounds (*S*)-12A and (*S*)-11F_2BTFO$_1$M$_7$ is presented. The tolane compound (*S*)-11F_2BTFO$_1$M$_7$ has the following phase sequence [9]:

C 46·4 S_C^* 100·6 TGB_C 101·3 TGB_A 104·2 N* 111·9 BP 112·7 I.

Again the complete miscibility of the TGB phases confirms our previous assignment. Furthermore, it is noteworthy that in spite of its small temperature interval, the TGB_C phase of compound (*S*)-11F_2BTFO$_1$M$_7$ is stable up to a dilution of at least 40 per cent.

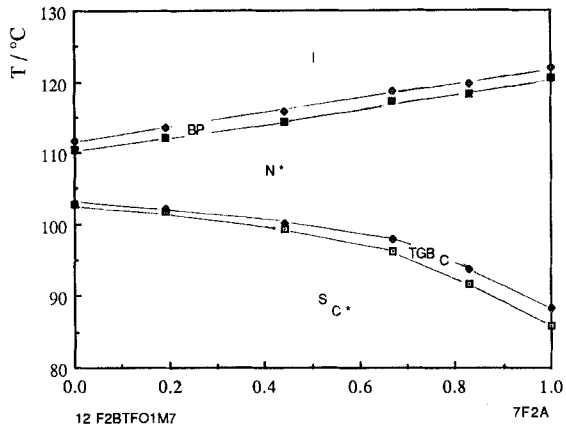

Figure 5. Binary phase diagram between (*S*)-7F_2A on the right and (*S*)-12F_2BTFO$_1$M$_7$ on the left.

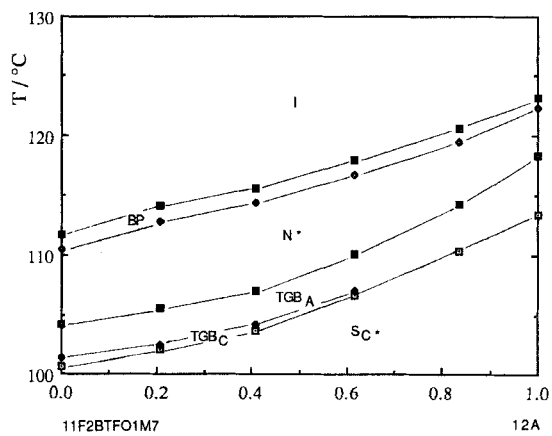

Figure 6. Binary phase diagram between (*S*)-12A on the right and (*S*)-11F_2BTFO$_1$M$_7$ on the left.

As a concluding summary of the phase assignment studies, the phase diagrams of the three series are given in figures 1, 2 and 3.

4. X-ray studies

X-ray scattering experiments were performed on powder or partially aligned samples. The samples were sealed in 1 mm Lindemann capillaries, whereby the shearing on filling the capillaries caused a partial orientation. We used CuK_α radiation from a Rigaku 18 kW rotating anode source. The detector used was a two-dimensional Mar-Research image plate detector coupled to a Digital Vax 3100 station. The detector consisted of an imaging plate with a diameter of 180 mm and a division into 1200×1200 pixels whereby the incoming radiation creates metastable electron states which can subsequently be read out by a He–Ne laser. The stimulated luminescence thus produced is linearly proportional to the radiation exposed. The distance between detector and sample was 1180 mm. The temperature was controlled up to a precision

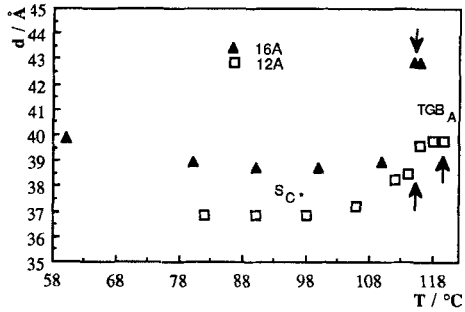

Figure 7. Layer spacing versus temperature for compounds 12A and 16A.

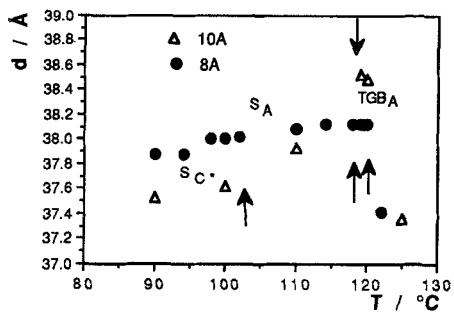

Figure 8. Layer spacing versus temperature for compounds 8A and 10A.

of 0·1 °C. With this set-up, no peak resolution studies could be performed, but it provided a qualitative analysis of the layered character of the TGB phases and gave the layer spacings in the smectic phases in general.

Four members of the *n*A series were studied with the following phase sequences:

16A: S_C^* TGB_A I;
12A: S_C^* TGB_A N* I;
10A: S_C^* S_A TGB_A N* I;
8A: S_A TGB_A N* I.

In the case of 16A, we observed a decrease of the layer spacing with increasing temperature in the S_C^* phase (see figure 7). Only at the phase transition to the TGB_A phase did a sudden rise in the layer distance occur, indicating the presence of a TGB_A phase. At 42·8 Å, the layer distance is still remarkably lower than the calculated molecular length with the alkyl chains in an all-*trans*-conformation; this underlines the high conformational disorder. Using the layer distance in the TGB_A phase to calculate the tilt angle in the S_C^* phase, we obtain an apparent tilt angle of 25·3°.

For the shorter molecule 12A, the evolution of the layer spacing on going from the S_C^* to the TGB_A phase has a much smoother character. The calculated tilt angle in the S_C^* phase, again using the layer spacings for the TGB_A phase as standard, is 22°.

Compound 10A shows a rather similar behaviour of a smooth transition from the S_C^* to the S_A and the TGB_A phase (see figure 8). Surprisingly the layer distance in the S_A phase appears to lie between the layer distances for the TGB_A and S_C^* phases. Due to the lack of data points, however, no further conclusions can be drawn.

The layer spacings of compound 8A show only a very weak temperature dependence. In particular, no change can be observed upon its transition into the TGB_A phase, underlining the similarity of the layer structure in the two phases. Upon transition into the cholesteric phase, the reflections for the last two compounds (8A and 10A) broaden considerably. Also they become highly asymmetric on the larger q-value side of the reflection, as has been observed before [9]. The peak values themselves are diminished as compared to the preceding phases.

5. Helical pitch measurement

These measurements have been performed as previously reported [8, 9] on prismatic samples oriented in the Grandjean–Cano texture. The results are reported in figure 9 for the compounds 12A and $10F_2A$.

For the compound 12A (see figure 9 (*a*)), the helical pitch is very short in the cholesteric phase below the I–N* transition—less than 0·22 μm, giving ultraviolet selective reflection. The pitch smoothly augments on cooling, and there is no major singularity at the N*–TGB_A transition. The pitch in the TGB_A phase diverges at the approach of the S_C^* phase, and we have followed this divergence up to values higher than 4 μm. The variations are quite similar to those we have observed for the tolane compounds $11FBTFO_1M_7$ [8] and $10F_2BTFO_1M_7$ [9], with the same S_C^*–TGB_A–N* sequence.

For the compound $10F_2A$, (see figure 9 (*b*)), the pitch in the N* phase starts from 0·21 μm close to the isotropic phase, and increases up to 0·41 μm close to the N*–TGB_C transition. An important discontinuity (0·41 μm to 0·95 μm) occurs at the N*–TGB_C transition. In the TGB_C phase, it is possible to follow a divergence of the pitch up to 2 μm. All these variations, mainly the discontinuity, are similar to those observed for the tolane $12F_2BTFO_1M_7$ [9] which exhibits the same phase sequence, S_C^*–TGB_C–N*.

We finally state that these azobenzene compounds are very sensitive to light illumination which produces photo-isomerization of the azo group and is able to shift the transitions more than 10°C to lower temperatures. The experiments reported here have therefore been performed with a minimum of light intensity.

6. Electro-optic properties

Electro-optic properties were studied in the SSFLC configuration to evaluate response time, spontaneous polarization and tilt angle in one set-up [13]. Commercial cells (Unicam) complete with ITO and rubbed PVA layer were used. The set-up consisted of a Eurelco 604 wave generator, a Kohn-Hite 10 watt wide-band amplifier and a Scientific Instruments Signal Memory Recorder, together with an Olympus BH2 microscope and a Mettler FP82 hot stage [11].

Three members of each series were studied. Field dependent studies showed that the saturation plateau is only reached at rather high values of 30 to 40 V. Therefore for the temperature dependence studies, a constant field of 35 V was chosen, in most cases together with a constant frequency of 1 kHz. Due to non-uniform reorientation effects, the measurement only becomes frequency dependent below 10 Hz.

The values of the spontaneous polarization are quite high in all cases, as observed for many three-ring compounds, in particular when they exhibit TGB phases (see figure 10). No drastic effects are observed upon further substitution of the benzoic acid moiety with fluorine atoms. The plateau values for the remaining compounds are 106 nC cm^{-2}, 76 nC cm^{-2}, and 80 nC cm^{-2} for 16Fa, 10FA, and $18F_2A$, respectively.

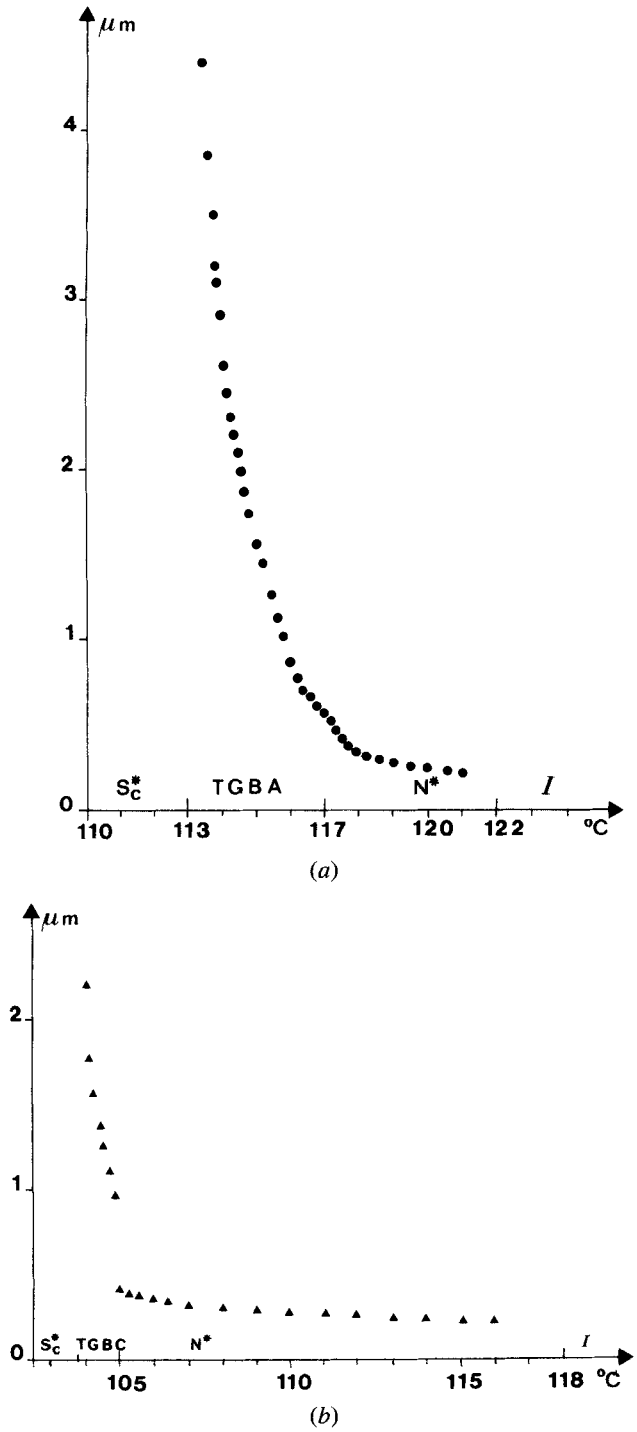

Figure 9. Helical pitch variations versus temperature for (*a*) 12A and (*b*) $10F_2A$.

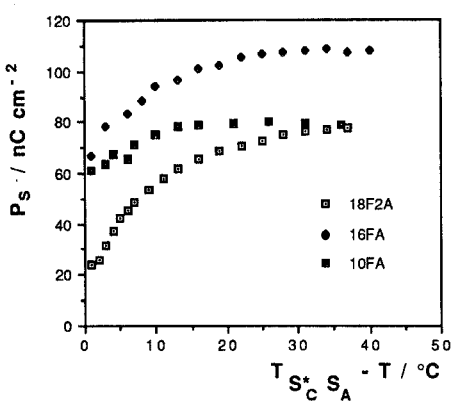

Figure 10. Spontaneous polarization versus $T_{S^*_C\text{–}S_A} - T$ ($V = 35$ V, $f = 3$ kHz).

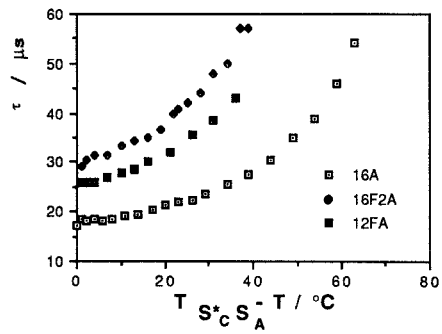

Figure 11. Response time versus $T_{S^*_C\text{–}S_A} - T$($f = 3$ kHz, $E = 5$ V μm^{-1}).

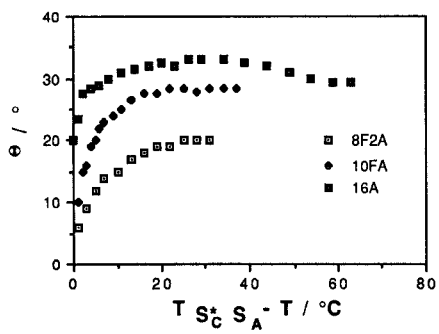

Figure 12. Tilt angle versus $T_{S^*_C\text{–}S_A} - T$.

The response times near the S_C^* to TGB transition are quite low—of the order 20 μs, but they increase substantially upon lowering the temperature for the longer chain compounds (see figure 11). Further fluoro-substitution leads to an increase in the response time, which is probably caused by a rise in rotational viscosity due to increased lateral interactions and steric hindrance. The tilt angles evolve in a similar way dependent on temperature, like the layer spacings from the X-ray measurements. The values for compound 16A stay approximately constant, probably due to improved alignment at higher temperatures. The tilt angles of compounds 10A and 12A decrease steadily and, as in the X-ray measurements, the S_C^*–S_A transition cannot be clearly distinguished for compound 10A. In the case of the electro-optic measurements, however, we must emphasize that we induce the molecular tilt due to the action of the electric field. The plateau tilt angle values for the remaining compounds are 32°, 32°, 27·5°, 30°, 31° and 19° for compounds 16FA, 12FA, 10FA, $18F_2A$, $12F_2A$ and $8F_2A$, respectively (see figure 12). When we compare the tilt angles obtained by optical methods with the angles obtained by X-ray measurements, we find that the latter values amount only to about 80 per cent of the optically determined values. This is a quite usual observation, the reason being the crude approximation made on calculating the tilt angles from the X-ray measurements and the fact that molecular moieties having different light dispersion properties such as the aromatic and the aliphatic parts of the molecules, might have different tilt angles towards the layer normals.

All reported values are characteristic of three-ringed compounds. In particular, they resemble closely the values obtained for the tolane compounds exhibiting TGB phases [8, 9].

7. Discussion

As anticipated from the close structural resemblence of the azobenzenes and tolanes, the TGB phase is found in all three series. This confirms the previously observed polarity rules for molecules forming TGB phases [9]. There are, however, some systematic deviations observed between the two classes when comparing directly the transition charts of the homologous series for the tolane and azobenzene series. We observe a preference of the azo-compounds for cholesteric and S_C^* phases. The TGB phases appear for molecules with a shorter alkyl chain length, and also the NAC tricritical point is shifted to shorter alkyl chain compounds. Bearing this in mind, the transition charts then become remarkably similar, and for the *n*A series, the NAC point coincides with the greatest thermal interval of existence for the TGB_A phase, as expected from theory. For the azobenzene series, this occurs with a 12 carbon alkyl chain, in contrast to a 16 carbon alkyl chain in the corresponding tolane series. In the nF_2A series, the preference for tilted phases is now too high. Only a small interval of TGB_C phase is found for the short alkyl chain compounds. The tolane series exhibits a rich polymorphism with TGB_A and TGB_C phases from the 10 carbon homologue onwards, but on comparing the series with the azobenzene series, they again resemble one another closely. The *n*FA series shows the same shift effect, with the compound with greatest TGB_A phase stability shifted from the 11 carbon compound in the tolane series to the 8 carbon compound in the azobenzene series.

As a conclusion, we note that the slight differences between the azobenzene and tolane moieties, notably the lower symmetry of the azobenzene and its increase in dispersive interactions due to the heteroatoms, which have practically no consequence for the crystal packing, play nevertheless an important role in fine tuning the position of the NAC point and thus the existence of the TGB phase.

8. Experimental

The infrared spectra were recorded on a Perkin–Elmer 783 spectrophotometer and the NMR spectra on a Bruker HW 270 MHz spectrometer.

The following examples are typical of the synthetic methods used to obtain the compounds indicated in the scheme in § 2 on Synthesis.

8.1.1. (*S*)-4-(*1-Methylheptyloxy*)-3-*fluoronitrobenzene*

To an ice-cooled solution of 4-nitro-3-fluorophenol (15·0 g, 95·5 mmol), (*R*)-2-octanol (12·42 g, 95·5 mmol) and triphenylphosphine (Ph_3P) (25·5 g, 95·5 mmol) in CH_2Cl_2 (200 ml) was added dropwise diethyl azodicarboxylate (DEAD) (18·3 g, 105·1 mmol). After stirring at room temperature overnight, the solution was filtered, evaporated and chromatographed on a silica gel column with heptane-ethyl acetate (2 : 1) as eluent. The product was a yellowish oil; yield: 25·0 g, 95 per cent. ^{1}H NMR ($CDCl_3$): 0·89 (t, 3 H, CH_2 of C_6H_{13}), 1·3 (m, 6 H, $3CH_2$), 1·37 (d, 3 H, CH_3–CH) 1·6–1·9 (m, 2 H), 4·6 (m, 1 H CH–CH_3), 7 (t, 1 H arom.), 8 (d, $J = 8$ Hz, 2 H arom.).

8.1.2. (*S*)-4-(*1-Methylheptyloxy*)-3-*fluoroaniline*

(*S*)-4-(1-Methylheptyloxy)-3-fluoronitrobenzene (25·0 g, 92 mmol) was dissolved in ethyl acetate (300 ml) and 1 g of 10 per cent Pd/C was added. Then hydrogen was added under a slight pressure. Hydrogen consumption stopped after about 5 h, after which the catalyst was filtered off and the solvent evaporated. The resulting oil was used without further purification. Yield 22·0 g, 99 per cent. ^{1}H NMR ($CDCl_3$): 0·89 (t, 3H, CH_2 of C_6H_{13}), 1·3 (m, 6 H, $3CH_2$), 1·36 (d, 3 H, CH_3–CH), 1·6–1·8 (m, 2 H), 4·05 (s, 2 H, NH_2), 4·3 (m, 1 H, CH–CH_3), 6·9 (t, 1 H arom.), 7·5 (d, $J = 8$ Hz, 2 H arom.).

8.1.3. (*S*)-4-(*1-Methylheptyloxy*)-3-*fluoro-4'-hydroxyazobenzene*

To an ice-cooled solution of (*S*)-4-(1-methylheptyloxy)-3-fluoroaniline (22·0 g, 91·7 mmol) in a mixture of dioxan (160 ml), concentrated hydrochloric acid (20 ml) and water (100 ml) was added slowly a solution of $NaNO_2$ (6·35 g, 91·7 mmol) in water (15 ml). After stirring at 0°C for another 2 h, the solution was transferred into a dropping funnel and added drop by drop to an ice-cooled solution of phenol (8·7 g, 91·7 mmol), NaOH (3·68 g, 91·7 mmol) and Na_2CO_3 (11 g) in water (120 ml) during about 1·5 h. After stirring for another 1·5 h, the solution was neutralized with concentrated hydrochloric acid, water and crushed ice and the product extracted three times into diethyl ether. Evaporation of the solvent and purification by chromatography on silica gel using a mixture of heptane–ethyl acetate (9 : 1) as eluent gave the pure product in a yield of 25·7 g, 81 per cent (orange crystals). ^{1}H NMR ($CDCl_3$): 0·89 (t, 3 H, CH_2 of C_6H_{13}), 1·29 (m, 6 H, $3CH_2$), 1·38 (d, 3 H, CH_3–CH), 1·6–1·8 (m, 2 H), 4·5 (m, 1 H, CH–CH_3), 5·6 (s, 1 H, OH), 6·9 (t, 1 H arom.), 7·5 (d, $J = 8$ Hz, 2H arom.). IR (Nujol): 3400, 1600, 1590, 1263, 830 cm^{-1}.

8.1.4. (*S*)-4-(*1-Methylheptyloxy*)-3-*fluoro-4'-(4-decyloxybenzoyloxy)azobenzene*

To a solution of (*S*)-4-(1-methylheptyloxy)-3-fluoro-4'-hydroxyazobenzene (344 mg, 1 mmol) in CH_2Cl_2 was added DCC (230 mg, 1·2 mmol), DMAP (20 mg) and 4-decyloxybenzoic acid (278 mg, 1 mmol). The mixture was stirred at room temperature overnight, filtered, the solvent evaporated and the product purified by chromatography over silica gel using toluene as eluent. In addition the final product was recrystallized from absolute ethanol, yielding 0·35 g, 58 per cent. ^{1}H NMR ($CDCl_3$): 0·88 (t, 3 H, CH_2 of C_6H_{13}), 1·25 (m, 6 H, $3CH_2$), 1·31 (d, 3 H, CH_3–CH), 1·6–1·8 (m, 4 H, $2CH_{2\beta}$), 4·05

(t, 2H, OCH_2), 4·5 (m, 1H, CH–CH_3), 6·9 (t, 1H arom.), 7·8–8·2 (4d, $J = 8$ Hz, 8H arom.). IR (Nujol): 1732, 1650, 1610, 1209, 830, 752 cm^{-1}.

The authors would like to express their gratitude to P. Barois and R. Bernon for their meticulous help during the performance of the X-ray experiments and to V. Faye and A. Babeau for DSC measurements and infrared spectra.

References

[1] De Gennes, P. G., 1972, *Solid St. Commun.*, **10,** 753.
[2] Renn, S. R., and Lubensky, T. C., 1988, *Phys. Rev.* A, **38,** 2132.
[3] Renn, S. R., and Lubensky, T. C., 1991, *Molec. Crystals liq. Crystals*, **209,** 349.
[4] Renn, S. R., 1992, *Phys. Rev.* A, **45,** 953.
[5] Goodby, J. W., Waugh, M. A., Stein, S. M., Chin, E., Pindak, R., and Patel, J. S., 1989, *Nature, Lond.*, **337,** 449.
[6] Goodby, J. W., Waugh, M. A., Stein, S. M., Chin, E., Pindak, R., and Patel, J. S., 1989, *J. Am. chem. Soc.*, **111,** 8119.
[7] Lavrentovich, O. D., Nastishin, Y. A., Kulishov, V. I., Narkevich, Y. S., Tolochko, A. S., and Shiyanovskii, S. V., 1990, *Europhysics Lett.*, **13,** 313.
[8] Bouchta, A., Nguyen, H. T., Achard, M. F., Hardouin, F., Destrade, C., Twieg, R. J., Maaroufi, A., and Isaert, N., 1992, *Liq. Crystals*, **12,** 575.
[9] (*a*) Nguyen, H. T., Bouchta, A., Navailles, L., Barois, P., Isaert, N., Twieg, R. J., Maaroufi, A., and Destrade, C., 1992, *J. Phys. II, Paris*, **2,** 1889. (*b*) Navailles, L., Barois, Ph., and Nguyen, H. T., 1993, *Phys. Rev. Lett.*, **71,** 545.
[10] Kitaigorodskij, A. I., *Organic Crystal Chemistry* (Consultants Bureau, N.Y.).
[11] Nabor, M. F., Nguyen, H. T., Destrade, C., Marcerou, J. P., and Twieg, R. J., 1991, *Liq. Crystals*, **10,** 785.
[12] Kelly, S. M., 1989, *Helv. chim. Acta*, **72,** 594.
[13] Clark, N. A., and Lagerwall, S. T., 1980, *Appl. Phys. Lett.*, **36,** 889.